Symmetry-allowed phase transitions realized by the two-dimensional fully frustrated *XY* class

Petter Minnhagen,[1] Beom Jun Kim,[2] Sebastian Bernhardsson,[1] and Gerardo Cristofano[3]
[1]*Department of Physics, Umeå University, 901 87 Umeå, Sweden*
[2]*Deparment of Physics, Sungkyunkwan University, Suwon 440-746, Korea*
[3]*Department of Physics, University of Naples, 80126 Naples, Italy*
(Received 28 October 2008; published 21 November 2008)

A two-dimensional (2D) fully frustrated *XY* (FF*XY*) class of models is shown to contain a different ground state in addition to the checkerboard ground states of the standard 2D FF*XY* model. The spin configuration of this additional ground state is obtained. Associated with this ground state there are additional phase transitions. An order parameter accounting for these transitions is proposed. The transitions associated with this order parameter are suggested to be similar to a 2D liquid-gas transition which implies Z_2 Ising-type transitions. This suggests that the class of 2D FF*XY* models belongs within a $U(1)\otimes Z_2\otimes Z_2$ designation of possible transitions, which implies that there are seven different possible single and combined transitions. Monte Carlo (MC) simulations for the generalized fully frustrated *XY* model on a square lattice are used to investigate which of these possibilities can be realized in practice: five of the seven are encountered. Four critical points are deduced from the MC simulations: three are consistent with central charge $c=3/2$ and one is consistent with $c=1$. The implications for the standard 2D FF*XY* model are discussed in particular with respect to the long-standing controversy concerning the characteristics of its phase transitions.

DOI: 10.1103/PhysRevB.78.184432 PACS number(s): 75.10.−b, 64.60.Cn, 74.50.+r

I. INTRODUCTION

The two-dimensional (2D) fully frustrated *XY* (FF*XY*) model describes a 2D Josephson-junction array in a perpendicular magnetic field with the strength of the magnetic field corresponding to one magnetic-flux quanta for every second plaquette of the array. The phase transitions of this model on a square lattice have been the subject of a long controversy.[1–8] The emerging canonical picture is that the model has two relevant phase ordering symmetries: an angular $\mathcal{U}(1)$ symmetry and a Z_2-chirality symmetry.[9–11] As a consequence, the model has often been assumed to belong within the designation $\mathcal{U}(1)\otimes Z_2$.[2–4,12] The controversial questions have been: does the model undergo a single combined transition or two separate transitions, and if the latter, in which order do the transitions occur? The emerging consensus is two separate transitions: as the temperature is increased first a Kosterlitz-Thouless (KT) transition associated with the angular $\mathcal{U}(1)$ symmetry and then at a slightly higher temperature a Z_2-chirality transition.[1] The cause of the controversy can, retrospectively, be attributed to the fact that the two transitions are extremely close in temperature.

We generalize here the 2D FF*XY* model into a wider 2D FF*XY* class of models by changing the nearest-neighbor interaction in such a way as to keep all symmetries. This generalized 2D FF*XY* class is shown to contain an additional ground state. The existence of this additional ground state leads to a phase diagram containing four sectors.[13] We show here that it has seven different phase-transition lines and four multicritical points. We use Monte Carlo (MC) simulations to establish the characters of the transitions of this phase diagram. Our simulations suggest that three of the critical points are consistent with the central charge $c=3/2$ and one with $c=1$.

In Sec. II we define the 2D FF*XY* model, and in Sec. III we describe the structure of the additional ground state. In Sec. IV we propose an order parameter associated with the transition into the additional ground state. In Sec. V we give the results for the various phase transitions obtained from Monte Carlo simulations and determine the character of the four multicritical points by invoking a relation between the central charge c and the bulk critical indices. In Sec. VI we discuss the original 2D FF*XY* model in view of our results. We also comment on related models not contained within the class of fully frustrated *XY* model discussed in the present investigation. Finally, some concluding remarks are given in Sec. VII.

II. GENERALIZED FULLY FRUSTRATED *XY* MODEL

The Hamiltonian which defines the 2D fully frustrated *XY*-class models on an $L\times L$ square lattice is given by

$$H=\sum_{\langle ij\rangle} U(\phi_{ij}\equiv\theta_i-\theta_j-A_{ij}), \tag{1}$$

with $\phi_{ij}\in[-\pi,\pi]$, where the sum is over nearest-neighbor pairs. The phase angle θ_i for the ith site at the lattice point (x_i,y_i) satisfies the periodicity $\theta_{i+L\hat{x}}=\theta_{i+L\hat{y}}=\theta_i$. The magnetic bond angle A_{ij} is defined as the line integral along the link from i to j, i.e., $A_{ij}\equiv(2\pi/\Phi_0)\int_i^j\mathbf{A}\cdot d\mathbf{l}$ with the magnetic vector potential $\mathbf{A}$ for the uniform magnetic field $\mathbf{B}=B_0\hat{z}$ in the z direction. With the Landau gauge taken, $A_{ij}=2\pi f x_i$ for the vertical link and $A_{ij}=0$ for the horizontal one, where the frustration parameter f measures the average number of flux quanta per plaquette. The fully frustrated case corresponds to $f=1/2$ with a half flux quantum per plaquette on the average. The Boltzmann factor, which determines the thermodynamic properties, is given by $\exp(-H/T)$ where T is the temperature. The interaction potential $U(\phi)=U(\phi\pm 2\pi)$ is periodic in 2π and is quadratic to lowest order in ϕ so that $U(\phi)\sim\phi^2$. These conditions for the interaction potential defines the class; the members of this class are distinguished by the

 ©2008 The American Physical Society

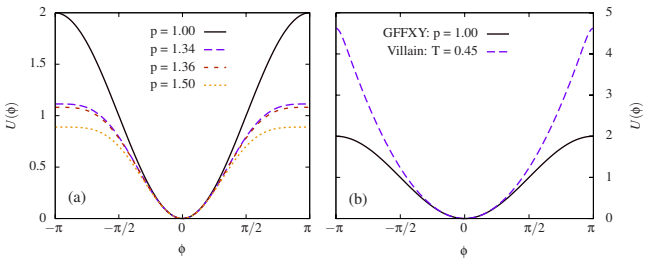

FIG. 1. (Color online) Interaction potentials $U(\phi)$ in Eq. (2) at various values of p are compared in (a). The standard XY model corresponding to $p=1$ is also compared with the Villain interaction potential in (b). All interactions have the same symmetry and have the identical quadratic form at small ϕ.

explicit form of the interaction potential $U(\phi)$. If the relevant symmetry class is $\mathcal{U}(1)\otimes Z_2$, then in principle three transitions are possible: separate $\mathcal{U}(1)$ and Z_2 transitions or a merged $\mathcal{U}(1)\otimes Z_2$ transition. However, the number of allowed phase transitions for the FFXY class is much larger.[13] The implication is that by just changing the specific form of $U(\phi)$ within the FFXY class, one could encounter a plethora of phase transitions. In order to verify this, we choose a parametrization of $U(\phi)$ and find the phase transitions corresponding to this parametrization using Monte Carlo simulation techniques. This strategy was employed earlier in Ref. 13. The parametrization is of the form $U(\phi)$ where[14,15]

$$U(\phi) = \frac{2}{p^2}\left[1 - \cos^{2p^2}\left(\frac{\phi}{2}\right)\right] \tag{2}$$

and $p=1$ corresponds to the standard FFXY since $2[1-\cos^2(\phi/2)]=1-\cos(\phi)$. The members of the FF$XY$ class, which belong to this parametrization, were in Ref. 13 termed as the generalized fully frustrated XY (GFFXY) model. Figure 1(a) shows a sequence of interaction potentials $U(\phi)$.

To sum up, the 2D FFXY class that we discuss here is obtained from the standard 2D FFXY by generalizing the interaction potential within the allowed conditions: $U(\phi)$ is a monotonously increasing function in the interval $\phi\in[0,\pi]$, and $U(\phi)=U(\phi\pm 2\pi)$ is periodic in 2π and is quadratic to lowest order in ϕ so that $U(\phi)\sim\phi^2$. The GFFXY model is by construction contained within this class. The Villain interaction is also contained in this class.[9] In Fig. 1(b) the interaction potential for the standard XY model $U(\phi)=1-\cos(\phi)$ is compared to the one for the Villain model at the KT transition $(T=0.45)$ $U(\phi)=-T\ln\{\Sigma_{n=-\infty}^{n=\infty}\exp[-(\phi-2\pi n)^2/2T]\}$.[1,9] The 2D FF$XY$ model with the Villain interaction has the same phase-transition scenario as the usual 2D FFXY model, i.e., a $\mathcal{U}(1)$ KT transition followed by a Z_2 transition (still extremely close together but a little less close than for the standard 2D FFXY model).[1] Is this true for all models within the FFXY class? The answer is no.[13] The reason is, according to us, connected to the appearance of an additional ground state.

III. GROUND STATE

Let us first consider the ground state for the standard 2D FFXY model on a square lattice. The spin configuration corresponding to the ground-state checkerboard is given in Fig. 2(a).[11] A square with (without) a flux quanta is denoted by + (−). The arrows give the spin directions and the thick (thin) links are the links with (without) magnetic bond angles π (0) modulo 2π. In this configuration all the links contribute the same energy $U(\frac{\pi}{4})$ to the ground state. Thus the energy for the four links constituting an elementary square is in this configuration $4U(\frac{\pi}{4})$. The broken symmetry of the free energy for $T=0$ is directly related to the fact that in order to change + to − squares in Fig. 2(a), by continuously turning the spin directions from one ground state to the other, an increase in the energy is required by a finite amount for a number of links. This required number of links goes to infinity with the size of the system; the two ground states are separated by an infinite energy barrier in the thermodynamic limit.

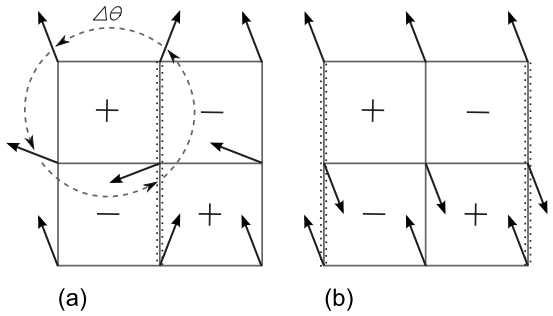

FIG. 2. Two groups of distinct ground states of the 2D GFFXY model. (a) When p is smaller than $p_c(\approx 1.3479)$, the gauge-invariant phase difference $\phi=\pi/4$ for all edges of a plaquette. (b) When $p>p_c$, one edge has $\phi=\pi$ while all the other three have $\phi=0$. The wiggled vertical lines denote the magnetic bond angles $A_{ij}=\pi$, arrows indicate phase values, and ± represent vortex charges.

The crucial point in the present context is that the ground state shown in Fig. 2(a) does not remain as the ground state for all values of p. As p is increased, the maximum link energy $U(\pi)$ decreases and at a particular value, $p_c>1$, the ground state switches to the spin configuration shown in Fig. 2(b). The energy for the links around a square for this configuration is given by $U(\pi)+3U(0)$. The critical value p_c is hence given by the condition $U(\pi)+3U(0)=4U(\frac{\pi}{4})$, leading to the determination

$$p_c = \sqrt{\frac{\ln(3/4)}{2\ln(\cos(\pi/8))}} = 1.3479. \tag{3}$$

The ground state for $p>p_c$ shown in Fig. 2(b) has the property that an infinitesimal change of the middle spin is enough to flip between the two checkerboard patterns [switching between + and − in Fig. 2(b)]. Thus there is no barrier between these two checkerboard patterns for $p>p_c$. This means that the broken symmetry of the free energy associated with the two possible checkerboard pattern states is restored. However, there is a different infinite barrier between the two degenerate ground states on opposite sides of p_c; continuously turning the spins to change from the spin configuration in Fig. 2(a) to the spin configuration in Fig. 2(b) requires an infinite energy.

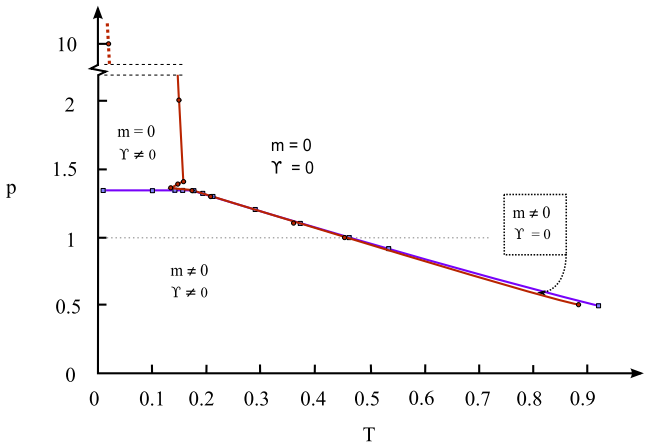

FIG. 3. (Color online) Phase diagram of the 2D GFF*XY* model in the (p,T) plane. The staggered magnetization m and the helicity modulus Y give us all four combinations, all of which are realized in the phase diagram. The horizontal dotted line at $p=1$ corresponds to the standard FF*XY* model which has two distinct and extremely close transitions.

IV. ORDER PARAMETERS

In order to characterize the phase-transition properties of the 2D GFF*XY* model, one needs to identify a set of order parameters with which all possible transitions can be characterized.

The checkerboard pattern is usually associated with a Z_2-chirality symmetry. For $T=0$ this symmetry is reflected in the existence of two degenerate ground states (the two checkerboards) separated by an infinite energy barrier. The corresponding order parameter is related to the staggered magnetization m defined as[10]

$$m = \left\langle \left| \frac{1}{L^2} \sum_{l=1}^{L^2} (-1)^{x_l+y_l} s_l \right| \right\rangle, \tag{4}$$

where $\langle \cdots \rangle$ is the ensemble average and the vorticity for the lth elementary plaquette at (x_l,y_l) is computed from $s_l \equiv (1/\pi)\Sigma_{\langle ij\rangle \in l}\phi_{ij} = \pm 1$ with the sum taken counterclockwise around the given plaquette. The corresponding broken symmetry is reflected in the following way: for any finite system the quantity $\frac{1}{L^2}\Sigma_{l=1}^{L^2}(-1)^{x_l+y_l}s_l$ can, with finite probability, acquire any value in the range $[-1,1]$ allowed by the model. However, in the thermodynamic limit $L=\infty$ only values in either the range $[-1,0]$ or the range $[0,1]$ can be acquired. This means that the order parameter $\mathcal{O}=\langle \frac{1}{L^2}\Sigma_{l=1}^{L^2}(-1)^{x_l+y_l}s_l\rangle$ in the thermodynamic limit can only take on the two values $\mathcal{O}=\pm m$. The probabilities for the two values are equal but they are separated by an infinite free-energy barrier. This is equivalent to saying that the order parameter $\mathcal{O}$ has a Z_2 symmetry which is broken. In the broken-symmetry region $m \neq 0$ whereas when the symmetry is unbroken $m=0$. Figure 3 shows the phase diagram in the (T,p) plane. As seen $m \neq 0$ corresponds to a finite region of this plane.

For $T=0$ and $p=p_c$, the two ground states in Figs. 2(a) and 2(b) are degenerate and are separated by an infinite energy barrier. For $T>0$ this should instead take the form of an infinite free-energy barrier in the thermodynamic limit, separating values that a local order parameter can acquire. To this end one needs to identify an appropriate local order parameter. Such a possible order parameter is the defect density n_k defined by

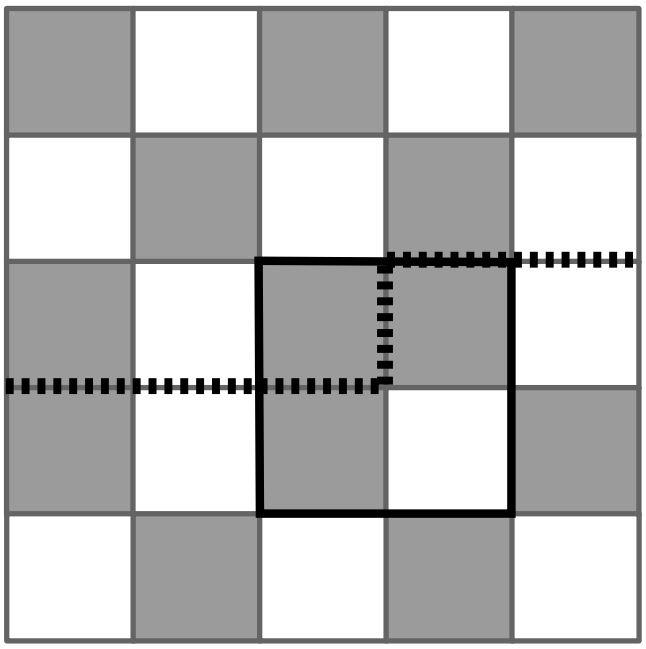

FIG. 4. Two checkerboard states with the boundary between them (denoted by a thick dotted line). A kink exists where the boundary makes a 90° turn, and the kink density n_k is measured by Eq. (5). For the four plaquettes surrounded by thick full line, $|s_t|=1$, whereas all other four plaquettes have even number of vortices and thus $|s_t|=0$.

$$n_k = \left\langle \frac{4}{L^2} \sum_{t=1}^{L^2/4} |s_t| \right\rangle, \tag{5}$$

where the square lattice has been divided into $\frac{L^2}{4}$ squares numerated by t where each consists of four elementary plaquettes. Here s_t is the sum of the phase difference around four-plaquettes $s_t \equiv (1/\pi)\Sigma_{\langle ij\rangle \in t}\phi_{ij}$ which means that $|s_t|$ can be 0, 1, or 2. Thus the defect density can be described in the following way: think of the elementary plaquettes as being either black $(s=1)$ or white $(s=-1)$. There are always equally many black and white squares. The defect density measures the average difference in the number of white and black squares contained in four-plaquettes. Obviously the checkerboard ground state corresponds to a zero defect density $n_k=0$. However, for a finite temperature the checkerboard ground state may contain a kink. This situation is illustrated in Fig. 4, starting from a checkerboard pattern. The thick dotted line is a boundary between the two possible checkerboard patterns. The 90° turn of this line is associated with a four-plaquette with $s_t=1$ which is denoted as thick solid line surrounding the four elementary plaquettes in Fig. 4. Thus a kink corresponds to a defect with $|s|=1$ according to our definition. The defect density defined here can be regarded as a generalization of the kink concept since it does

not rest on the possibility of uniquely identifying domain boundaries. Thus the defect density remains as a well-defined concept even when the checkerboard symmetry is completely restored and $m=0$. The ground state shown in Fig. 2(b) is an example of a situation when $m=0$ because switching between + and − in Fig. 2(b) does not involve passing any energy barrier. Thus the defect density remains finite as T is lowered toward zero for any $p>p_c$. Consequently, the ground state in Fig. 2(b) corresponds to a finite defect density $n_k>0$. It is also obvious that the defect density is monotonously increasing with T.

A phase transition associated with this order parameter is signaled by either a discontinuous or a nonanalytical behavior of n_k as a function of T and p. The defect density makes a discontinuous jump from zero to a finite value at p_c in the limit of small temperatures, and these two values are separated by an infinite energy barrier; the point $(p,T)=(p_c,0)$ is the starting point of a phase-transition line (see Fig. 3). On this phase-transition line the order parameter n_k can only take on two values. These two values are equally probable but are separated by an infinite free-energy barrier. Thus the order parameter n_k on this phase-transition line possesses a Z_2 symmetry which is broken.

One should note that in the case of n_k the infinite free-energy barrier between two different but equally probable values of n_k only resides on well-defined lines in the (p,T) plane, whereas the infinite barrier for the chirality transition resides on an area of the (p,T) plane (see Fig. 3). Thus the phase transition associated with the defect density n_k is more akin to a liquid-gas transition in the pressure temperature plane; the order parameter is the density difference on the two sides of the transition line and the infinite free-energy barrier only exists precisely on the transition line.

The $\mathcal{U}(1)$ symmetry in 2D is at most "quasibroken" because of the Mermin-Wagner theorem.[16] As a consequence the corresponding phase transitions cannot be described by a local order parameter. Instead the phase transitions can be monitored by the increase in the free energy caused by a uniform twist δ of the spin angles across the system. Expanding the free energy $F(\delta)$ for small values of δ to lowest orders gives

$$F(\delta) = Y\frac{\delta^2}{2} + Y_4\frac{\delta^4}{4!}. \tag{6}$$

Here, Y is the helicity modulus. It is finite in the low-temperature phase and zero in the high-temperature phase.[17] Y_4 is the fourth-order modulus and can be used to verify that the helicity modulus Y makes a discontinuous jump to zero at the transition.[18] This discontinuous jump is a key characteristics of the KT transition.[19,20]

V. PHASE DIAGRAM AND PHASE TRANSITIONS

In Ref. 13 the phase transitions associated with the $\mathcal{U}(1)$ symmetry and the Z_2-chirality symmetry were investigated. The corresponding phase diagram is reproduced in Fig. 3. This phase diagram has four sectors corresponding to all four possible combinations of transitions for a combined symmetry $\mathcal{U}(1)\otimes Z_2$. The four sectors are characterized by the four possible combinations $(\Upsilon,m)=(0,0)$, $(0,\neq 0)$, $(\neq 0,0)$, and $(\neq 0,\neq 0)$. The dashed horizontal line at $p=1$ in Fig. 3 corresponds to the usual FFXY model. In this case the phase $(\Upsilon\neq 0, m=0)$ is not realized.[13]

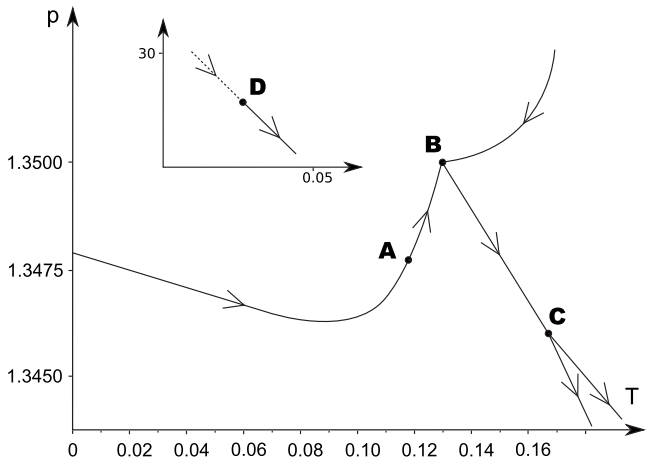

FIG. 5. Magnified phase diagram near $p_c\approx 1.3479$ (compare with Fig. 5). There are in total four multicritical points termed as A, B, C, and D (see text). The critical point D shown in the inset occurs at much higher p and lower T.

In the present paper we use all the three-order parameters described in Sec. IV together with Monte Carlo simulations in order to deduce the nature of the various phase boundaries.

Figure 5 gives a sketch of the resulting "horizontal" phase boundary in Fig. 3. In this blown up scale one finds that it has one maximum and one minimum as well as three multicritical points ending three distinct phase lines. The critical points are denoted by A, B, and C. A fourth multicritical point is found along the "vertical" phase line at much higher p and lower T (see Figs. 3 and 5). Let us first consider the phase boundary from $T=0$ to the critical point A. Across this first section of the phase boundary the phase transition associated with the defect density n_k is of the first order. Figure 6(a) illustrates the discontinuous change in the defect density n_k. The defect-density histogram along this phase line has two distinct values of equal probability which remain distinct in the large-L limit. An example is given in Fig. 6(b). For a given temperature T, the lower value corresponds to the low-p phase and the higher to the high-p phase. As pointed out above, this is analogous to the density for a liquid-gas transition. Note that for $T=0.1$ the p value for the first-order line is lower than $p_c(0)$. However, as T is further increased, the p value for the first-order line increases. Finally, at a critical temperature T_{cA} the density difference vanishes with increasing system size. This is the signature of the critical point A which is hence the critical point ending the first-order transition line for the defect density. Thus the critical point A is analogous to the critical point ending the first-order line for a gas-liquid transition. Figure 6(c) shows the defect-density histogram close to the critical point; at the critical point the free-energy barrier between the two phases is L independent. This means that the ratio between the maximum and minimum in the kink-density histogram should also be size independent, whereas

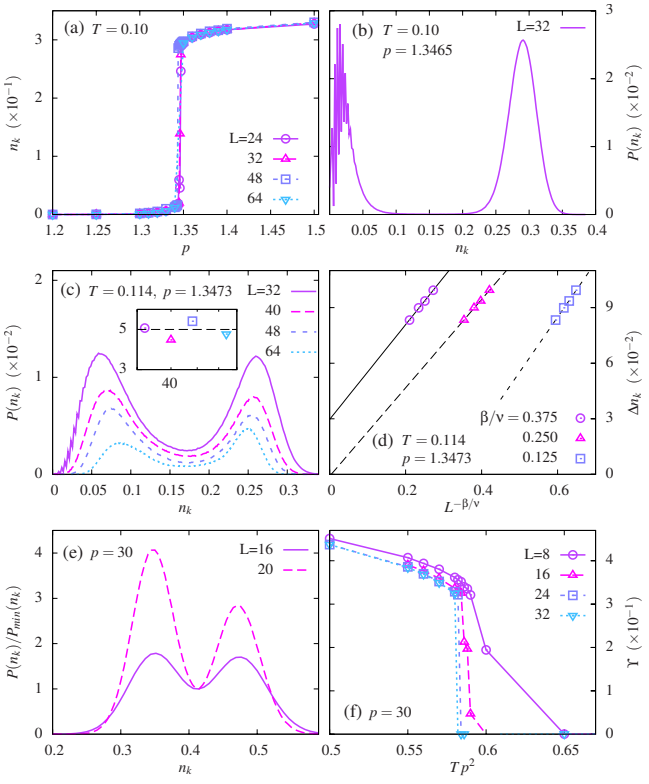

FIG. 6. (Color online) (a) First-order transition of n_k at $T=0.1$. (b) Two valued probability distribution $P(n_k)$ at the abrupt change in (a). (c) $P(n_k)$ at the critical point A. The inset shows that the ratio $P_{\max}/P_{\min}$ is to good approximation finite and independent of L. (d) Finite size scaling, $\Delta n_k \sim L^{-\beta/\nu}$, is consistent with $\beta/\nu=1/4$. (e) $P(n_k)$ for a large-p value above the critical point D. The figure illustrates that $P_{\max}/P_{\min} \to \infty$ with increasing system size. (f) Helicity modulus transition at the same T and p as in (e), indicating a joint first-order transition.

it increases (decreases) for lower (higher) temperatures.[21] This size-independence is fulfilled to a good approximation of the T value in Fig. 6(c). At the critical point the defect-density difference Δn_k [the difference between the two maxima in Fig. 6(c)] should vanish with size as $\Delta n_k \sim L^{-\beta/\nu}$.[21] The Δn_k size scaling is shown in Fig. 6(d) and is consistent with an exponent $\beta/\nu=0.25$. One can express this exponent in terms of the central charge c as $\beta/\nu=c/4$.[22,23] The central charge c is coupled to the symmetry of the order parameter. The defect density, the staggered magnetization, and the magnetization for the 2D Ising model can all acquire precisely two distinct values with equal probability separated by an infinite energy barrier. The broken symmetry reflected by these order parameters does hence have a Z_2 character, and the phase transitions are Ising-type. The central charge is $c=1/2$ for 2D Ising-type transitions. If the order parameter on the other hand is a 2D vector then the symmetry is $U(1)$ (which means that the order parameter with equal probability has the same magnitude at any direction, but all these possibilities are separated by an infinite energy barrier) and the central charge is $c=1$. Provided that our three-order parameters cover all possibilities, then a phase transition can *a priori* be any combination of single and joint transitions involving these order parameters and is hence contained within

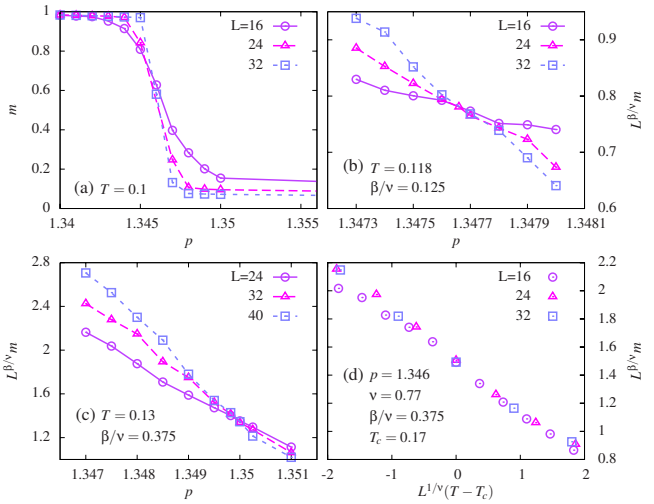

FIG. 7. (Color online) (a) The staggered magnetization $|m|$ at $T=0.1$. (b) Size scaling $|m| \sim L^{-\beta/\nu}$ for $T=0.118$ (just above point A), consistent with $\beta/\nu=1/8$. (c) Size scaling between points B and C, consistent with $\beta/\nu=3/8$. (d) Size scaling $m=L^{-\beta/\nu}f[(T-T_{cC})L^{1/\nu}]$ for the critical point C. Good scaling collapse obtained for $T_{cC} \approx 0.17$ with $\nu \approx 0.77$ [from Fig. 8(d)] and $\beta/\nu=3/8$.

the designation $\mathcal{U}(1) \otimes Z_2 \otimes Z_2$. This implies that the central charge can have the four values of $c=1/2$, 1, 3/2, and 2. Here a Z_2 transition corresponds to $c=1/2$, an individual KT transition or a combined $Z_2 \otimes Z_2$ transition corresponds to $c=1$, the two possible combined $\mathcal{U}(1) \otimes Z_2$ transitions correspond to $c=3/2$, and a combined $\mathcal{U}(1) \otimes Z_2 \otimes Z_2$ corresponds to $c=2$. These possibilities are tested in Fig. 6(d) and single out $c=1$ or equivalently $\beta/\nu=1/4$. This means that among the four possible values only $c=1$ is consistent with the data. As will be explained below, the helicity modulus remains nonzero in this part of the phase diagram (compare to Fig. 3), and consequently this suggests that the critical point A reflects a combined $Z_2 \otimes Z_2$ defect-density and chirality transitions. The defect-density transition ends at the critical point A; as T is increased the free-energy barrier vanishes in the large-L limit. However, there is a second defect-density transition line for higher p values associated with a $\mathcal{U}(1) \otimes Z_2$ combined KT and defect-density transition, as illustrated in Figs. 6(e) and 6(f). This transition is first order for higher p and ends at a critical point D; for a T higher than the critical point D there is no defect-density transition, just as for the case of the critical point A.

Figure 7(a) illustrates the chirality transition along the same phase boundary. Up to the critical point A (see Fig. 5) the transition is of first order [see Fig. 7(a)]. The chirality transition cannot cease at the critical point A because for a fixed T the free-energy barrier between the $\mathcal{O}=\pm|m|$ always vanishes for a large enough p. There are then two possibilities: it can continue alone as a Z_2 transition or it can combine with the KT transition into a joint $\mathcal{U}(1) \otimes Z_2$ transition. To deduce which possibility is the correct one, we calculate the size scaling of $m \sim L^{-\beta/\nu}$ and decide which of the two possible symmetry-allowed values, $\beta/\nu=c/4=1/8$ or 3/8, is consistent with the data. Here we use standard size scaling and calculate $m(T,p)$ for a fixed T for a sequence of p which crosses the phase line. As seen in Fig. 7(b), a unique crossing

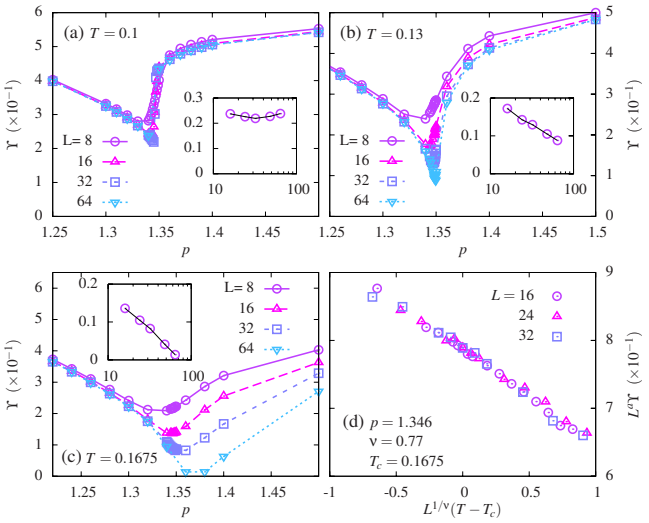

FIG. 8. (Color online) (a) The helicity modulus, Υ, across the phase line below point A. The inset shows that the minimum of Υ remains finite with increasing size. (b) Υ goes to zero for large sizes between B and C. (c) Same as (b) at point C. (d) Size scaling relation $\Upsilon = L^{-a} g\{[(T-T_{cC})L^{1/\nu}]$ with good collapse for $\nu \approx 0.77$ ($a \approx 0.63$ and $T_c \approx 0.1675$ are taken from Ref. 13).

point is to good approximation obtained for $\beta/\nu = 1/8$. From this we conclude that the chirality transition continues alone from the critical point A as a Z_2 transition. However as we further increase the temperature the character of the chirality transition changes; using the same procedure we instead find that the value $\beta/\nu = 3/8$ is consistent with the data [see Fig. 7(c)]. This is consistent with a joint $\mathcal{U}(1) \otimes Z_2$ KT-chirality transition. As we increase T further we come to the critical point C where the KT and chirality splits up into two separate transitions.[13] At this point it is possible to instead calculate the size scaling for a fixed p. The advantage is that we can use the standard size scaling form $m = L^{-\beta/\nu} f[(T - T_{cC})L^{1/\nu}]$. This again shows that the value $\beta/\nu = 3/8$ is consistent with the data. From this we deduce that there must exist a critical point B between A and C where the chirality transition merges with the KT transition.

Are these deductions consistent with the $\mathcal{U}(1)$ symmetry and the helicity modulus? We argued above that the transition from $T=0$ to the critical point A is associated with the $Z_2 \otimes Z_2$ symmetry. This presumes that the $\mathcal{U}(1)$ symmetry remains quasibroken on both sides of the transition, or equivalently, that the helicity modulus Υ is finite on both sides. This is illustrated in Fig. 8(a); the helicity modulus Υ has a minimum at the phase line. However, this minimum remains nonzero in the large-L limit, as illustrated by the inset of Fig. 8(a). Thus Υ makes (at most) a finite jump at the transition and the $\mathcal{U}(1)$ symmetry remains quasibroken. Next we argued that between the critical points B and C, the transition is a combined $\mathcal{U}(1) \otimes Z_2$-KT-chirality transition. This means that the helicity modulus must now vanish at the transition. This is illustrated in Fig. 8(b), which shows that the Υ minimum now vanishes in the large-L limit [compare inset of Fig. 8(b)]. Figure 8(c) shows the same construction close to the critical point C. The fact that Υ vanishes as a power law can be verified for the critical point C by instead varying T for fixed p. In these variables the critical point C obeys a standard scaling relation $\Upsilon = L^{-a} g\{[(T-T_{cC})L^{1/\nu}]$ which confirms the power-law decay of Υ, as opposed to the KT-universal jump signaling the isolated $\mathcal{U}(1)$ transition for the XY model [see Fig. 8(d)].[13] We also note that the obtained critical index $\nu \approx 0.77$ is consistent with the data for m in Fig. 7(d). It is also possible to use the fourth-order helicity modulus Υ_4 to determine the character of the $\mathcal{U}(1)$ transition.[18] In Ref. 13 it was found from the Υ_4 data that in the interval $1.346 \leq p \leq 1.35$, the character of the $\mathcal{U}(1)$ transition was consistent with a transition without a discontinuous jump in the helicity modulus Υ. This is consistent with a combined $\mathcal{U}(1) \otimes Z_2$ transition between the multicritical points B and C.

The following picture emerges: A and D end two first-order phase lines. A is associated with a $Z_2 \otimes Z_2$ transition with a central charge of $c=1$ and D with a $\mathcal{U}(1) \otimes Z_2$ transition with $c=3/2$. B and C are both associated with $\mathcal{U}(1) \otimes Z_2$ transitions and $c=3/2$ but are not end points of first-order lines.

VI. STANDARD 2D FFXY MODEL

The usual 2D FFXY model corresponds to the $p=1$ line in Fig. 3. The critical point C for the 2D FFXY class is the closest multicritical point to the actual phase transitions of the usual 2D FFXY model (compare to Fig. 5). The critical point C is characterized by the critical index $\nu \approx 0.77$ and the central charge $c=1.5$. A single Z_2 transition is characterized by $\nu=1$ and $c=0.5$. In all the earlier papers, in which it was putatively concluded that the 2D FFXY model has a joint transition, the apparent value of ν was in the interval $0.77 < \nu < 1$ (see Table I in Ref. 1). In particular in Ref. 5 the values of ν and c were independently determined and were given by $\nu = 0.80(4)$ and $c = 1.61(3)$. Thus the apparent multicritical point for the usual FFXY model appeared to have critical properties inconsistent with a single Z_2 transition and with critical ν values in between a single Z_2 transition and the real $\mathcal{U}(1) \otimes Z_2$ multicritical point C for the 2D FFXY class. Furthermore, the closeness of the ν and c values [$\nu \approx 0.77$ and $c=1.5$ for C, respectively, $\nu = 0.80(4)$ and $c = 1.61(3)$ obtained for the usual FFXY model in Ref. 5] suggests that the putative multicritical point found for the 2D FFXY model is an artifact of the closeness to the real critical point C for the 2D FFXY class.

The present consensus is that the 2D FFXY model undergoes two separate transitions, a KT transition at T_{KT} followed by a Z_2 transition at T_{Z_2} with $T_{\mathrm{KT}} < T_{Z_2}$.[1] In particular Korshunov in Ref. 8 gave a general argument which purportedly states that $T_{\mathrm{KT}} < T_{Z_2}$ should be true not only for the 2D FFXY model but also for the 2D FFXY class studied in the present work, provided that the interaction is such that its ground state is the broken-symmetry checkerboard state. This is in contradiction with the existence of the multicritical point C at $p < p_c$ (compare to Fig. 5) which corresponds to an interaction potential with a checkerboard ground state. We suggest that the reason for this fallacy of the argument is connected to the closeness to the $(m, Y) = (0, \neq 0)$ phase.

The most striking feature of the phase transition for 2D FFXY model is the closeness between T_{KT} and T_{Z_2}. The

phase diagram in Fig. 5 gives a scenario for which this feature becomes less surprising. The point is that the chirality and the KT transitions merge and cross as a function of p for the 2D GFFXY model. It then becomes more natural that for some values of p, the transitions can be extremely close. The value $p=1$, which corresponds to the usual FFXY model, happens to be such a value.

There are many other $\mathcal{U}(1)\otimes Z_2$ models related to the 2D FFXY model.[1] Although, our results only pertain to the 2D FFXY class defined in this paper, we note that to our knowledge, none of the phase diagrams for related models contains a crossing of the KT and an Ising-type transition. In a vast majority, the KT transition is always at lower temperature than the Ising-type transition or possibly merged. However, in the model in Ref. 24 the situation is reversed with the Ising-type transition below or merging with the KT transition. Also in this case a crossing is lacking. Because there is no crossing it is notoriously difficult to assert whether a merging takes place or the two transitions are only extremely close.[1] For example, the Ising-XY model was in Refs. 2, 4, and 12 found to contain such a line of merged transitions. However, more careful MC simulations in fact suggest that the transitions are extremely close but never merge along this line.[1] The point to note is that for our 2D GFFXY model the transitions *cross*, from which it directly follows that a real merging exists in this case. We believe that this crossing is intimately related to the appearance of the additional ground state.

VII. FINAL REMARKS

To sum up, we have found that the description of the phase diagram for the 2D FFXY class of models requires at least three distinct order parameters consistent with the proposed designation $\mathcal{U}(1)\otimes Z_2\otimes Z_2$. In addition to the usual KT $\mathcal{U}(1)$ transition and the chirality Z_2 transition, there is also a defect-density transition with Ising-type Z_2 character. Within our simple parametrization of the interaction $U(\phi)$, we have found that all combinations of transitions can be realized except for two: the single Z_2-defect transition and the fully combined $\mathcal{U}(1)\otimes Z_2\otimes Z_2$ transition. All the others are realized, i.e., the single Z_2-chirality transition, the single $\mathcal{U}(1)$ KT transition, the combined Z_2-defect and Z_2-chirality transitions, the combined Z_2 chirality and $\mathcal{U}(1)$ KT, and the combined Z_2-defect and the $\mathcal{U}(1)$ KT transitions. Since the GFFXY model is a subclass of the 2D FFXY class this means that at least five of the symmetry-allowed transitions can be realized. What about the remaining two? Here we speculate that a single Z_2 density transition will hardly be realized because it couples too strongly to the other transitions. However, one might imagine that there exists a potential $U(\phi)$ for which the two nearby critical points A and B are merged. This critical point would then correspond to a merged $\mathcal{U}(1)\otimes Z_2\otimes Z_2$ transition with central charge $c=2$.

We also note that Cristofano *et al.* in Ref. 25 argued from general symmetry considerations that the full symmetry of the FFXY model allows for $\mathcal{U}(1)\otimes Z_2\otimes Z_2$. The present results for the phase diagram of the 2D GFFXY model support this designation.

ACKNOWLEDGMENTS

P.M. and S.B. acknowledge support from the Swedish Research Council under Grant No. 621-2002-4135. B.J.K. acknowledges the support from the KRF under Grant No. KRF-2005-005-J11903.

[1] For a recent review, see M. Hasenbusch, A. Pelissetto, and E. Vicari, J. Stat. Mech.: Theory Exp. (2005) P12002.
[2] E. Granato, J. M. Kosterlitz, J. Lee, and M. P. Nightingale, Phys. Rev. Lett. **66**, 1090 (1991).
[3] J. Lee, J. M. Kosterlitz, and E. Granato, Phys. Rev. B **43**, 11531 (1991).
[4] J. Lee, E. Granato, and J. M. Kosterlitz, Phys. Rev. B **44**, 4819 (1991).
[5] E. Granato and M. P. Nightingale, Phys. Rev. B **48**, 7438 (1993).
[6] P. Olsson, Phys. Rev. Lett. **75**, 2758 (1995).
[7] E. H. Boubcheur and H. T. Diep, Phys. Rev. B **58**, 5163 (1998).
[8] S. E. Korshunov, Phys. Rev. Lett. **88**, 167007 (2002).
[9] J. Villain, J. Phys. C **10**, 1717 (1977).
[10] S. Teitel and C. Jayaprakash, Phys. Rev. B **27**, 598 (1983).
[11] T. Halsey, J. Phys. C **18**, 2437 (1985).
[12] M. P. Nightingale, E. Granato, and J. M. Kosterlitz, Phys. Rev. B **52**, 7402 (1995).
[13] P. Minnhagen, B. J. Kim, S. Bernhardsson, and G. Cristofano, Phys. Rev. B **76**, 224403 (2007).
[14] E. Domany, M. Schick, and R. H. Swendsen, Phys. Rev. Lett. **52**, 1535 (1984).
[15] A. Jonsson and P. Minnhagen, Phys. Rev. Lett. **73**, 3576 (1994).
[16] N. D. Mermin and H. Wagner, Phys. Rev. Lett. **17**, 1133 (1966).
[17] P. Minnhagen, Rev. Mod. Phys. **59**, 1001 (1987).
[18] P. Minnhagen and B. J. Kim, Phys. Rev. B **67**, 172509 (2003).
[19] D. R. Nelson and J. M. Kosterlitz, Phys. Rev. Lett. **39**, 1201 (1977).
[20] P. Minnhagen, Phys. Rev. B **24**, 6758 (1981).
[21] K. Binder and D. Heermann, *Monte Carlo Simulations in Statistical Physics*, 2nd ed. (Springer-Verlag, Berlin, 1992).
[22] D. S. P. Di Francesco and P. Mathieu, *Conformal Field Theories* (Springer-Verlag, New York, 1997).
[23] Our MC simulations give an *a posteriori* verification of this relation for the present model.
[24] B. Berge, H. T. Diep, A. Ghazali, and P. Lallemand, Phys. Rev. B **34**, 3177 (1986).
[25] G. Cristofano, V. Marotta, P. Minnhagen, A. Naddeo, and G. Niccoli, J. Stat. Mech.: Theory Exp. (2006) P11009.